Available online at www.sciencedirect.com
ScienceDirect
Journal of Molecular Catalysis A: Chemical 271 (2007) 105–116
JOURNAL OF MOLECULAR CATALYSIS A: CHEMICAL
www.elsevier.com/locate/molcata

Nature of the NiMoS catalyst edge sites: An atom in molecules theory and electrostatic potential studies

Yosslen Aray *, Jesús Rodríguez, Alba Beatriz Vidal, Santiago Coll

Centro de Química, IVIC, Apartado 21827, Caracas 1020 A, Venezuela

Received 17 November 2006; received in revised form 5 February 2007; accepted 12 February 2007
Available online 20 February 2007

Abstract

The nature of the active sites on the NiMoS catalyst was explored using the combination of the atoms in molecules theory and an electrostatic potential based methodology. Direct visualization of the basin of the outermost atoms of the studied NiMoS edge models has shown that the Mo atoms are practically covered by the outermost S atoms while the promoter Ni are the most accessible atoms to the exterior of the edges. Electrostatic potential mapping on the atomic border exposed to the exterior of the edge and adsorption of pyridine as the probe molecule have shown that the adsorption of a molecule containing the pollutant atoms strongly depends on two factors: the Lewis acidity of the site and the repulsive interaction of the incoming molecule with sulfur atoms impeding the free access to the site. In this sense, the main role of the promoter is to produce sulfur uncovered Lewis acid sites. Extraction of the outermost S atom creates a very strong Lewis acid site locate at uncovered Mo atoms.
© 2007 Elsevier B.V. All rights reserved.

Keywords: HDS; Atoms in molecules theory; Electrostatic potential; NiMoS; DFT

1. Introduction

Transition metal sulfides (TMS) belong to a very important class of catalysts characterized by being stable under strong conditions in hydrodesulfurization (HDS), hydrodenitrogenation (HDN) and hydrogenation reactions [1–3]. In these processes, the surfaces of the sulfides are reduced by sulfur elimination using large excess of hydrogen at temperature ranging from 573 to 673 K creating coordinatively unsaturated sites (CUS) or vacancies around the metals. CUS intervenes as an electron-withdrawing site whose properties may be regarded as a Lewis acid center interacting with electrodonating organic substrates [4–6]. The nature of these sites is suggested to be intimately related to the metal sulfur bond strength [4,5,7,8]. Basic studies support the view that differences in catalytic activities, are related to variations in the concentration of CUS (the Lewis acid sites), which in turn depend on the metal–sulfur bond strength [9–20]. Based on ab initio calculations [2,7], a bond energy model (BEM), which describes the variation in the metal–sulfur bond energies for all the transition metal sulfides was developed. It was found that the trends in the calculated bond energies follow closely the trend in the HDS activities. Nickel- (and cobalt) promoted Molybdenum sulfide catalysts have for many years been among the most important catalysts in refinery service. Studies using X-ray absorption fine structure (EXAFS) have established that the active Mo atom is present as small MoS_2-like nanostructures [21,22]. Adsorption and activity experiments [23,24] have revealed that the active sites reside at the edges of the MoS_2 structures and a recently high-resolution scanning tunneling microscopy (STM) and density-functional theory (DFT) studies [25] have shown that the MoS_2 nanoclusters adopt a hexagonal shape exposing two different types of edges, Mo edges covered with S monomers and fully sulfur-saturated S edges. On the other hand, the incorporation of nickel or cobalt into these edges significantly increases the activity of the catalyst [2,26,27]. Hydrogen species on the surface of catalyst is crucial to catalytic activity. In this sense, Ni facilitated the dissociation of H_2 by increasing the stability of the transition state and products for this reaction [28]. Under typical sulfidation conditions Ni prefers to incorporate into the metal edge. A fully Ni promoted metal edge tends to be not covered with sulfur atoms [27]. The addition of one sulfur atom on such a surface is an

* Corresponding author. Tel.: +58 212 504 1356; fax: +58 212 504 1350.
E-mail address: yaray@ivic.ve (Y. Aray).

1381-1169/$ – see front matter © 2007 Elsevier B.V. All rights reserved.
doi:10.1016/j.molcata.2007.02.016

endothermic process. On a partially promoted metal edge, sulfur atoms bond to the outermost Mo atoms and the promoter atoms tend to be uncovered.

The "*atoms in molecules theory*" (AIM) of Bader et al. is very useful to obtain the chemical information from the charge density [29–38]. AIM is a firm, rigorous and quantum mechanically well-defined theory based on observables such as the electron density or energy density fields. Most modern theories of bonding are based, in one way or another, on the partition of charge (or electronic density) among the different nuclear centers under study, usually by means of Mulliken-i.e., projected density of states in solid-analysis. In this way, an important amount of the interpretative models of chemical behavior are based on concepts that are known to be very badly defined, and to give answers extremely dependent on a whole hierarchy of approximations [36]. AIM provides a quantitative link between the total electron density (regardless of how it was generated: calculated or experimental) and the all important physical properties of a molecule, bypasses the wave function in the analysis. AIM is an orbital concept free methodology. In particular, it provides a rigorous definition of chemical bonds and geometrical structure for all types of molecules and solids and has proven useful in the analysis of physical properties of insulators, pure metals and alloys [32–36]. High-quality experimental densities of minerals [39–43], covalent [44], metallic [45], and molecular crystals [46–49] have been analyzed in terms of AIM concepts. Theoretical calculations on simple metals [35,50–52], alloys and intermetallic phases [53–57], molecular [52,58–60], covalent and ionic crystals have also been reported [36,43,44,52,61,62]. AIM also provides a rigorous topological and quantum mechanical definition of atoms that have been identified with the atom of chemistry. These atoms have shown to recover the essential notions associated with the atomic concept: (i) the atomic properties are characteristic and additive to yield the corresponding values for the total system; (ii) they are as transferable from one system to another as are the forms of the atoms in real space; that is, as transferable as are the atomic charge distribution. In particular, atomic and group properties predicted in this manner have been shown to recover the experimentally determined contributions to the volume, energy, polarizability, and magnetic susceptibility [25]. Additionally, the most agreeable feature of AIM probably is that it lends itself so well to visualization of the atoms using computer graphics. The connection between the topology of the electron density and the chemical and structural stability of isolated molecules and crystals has been well established [30,36,34,19,32,35,63]. Recently, the nature of the MoS_2 catalyst edge using AIM was reported [20]. Two interesting facts were observed: first, similar to the bulk case, the layers are bonded by S–S interlayer bonds and second, much bigger electron density on the graphs describing the Mo edge suggests to be the origin of the well-known easiness to create vacancies on the S edge. Additionally, it has found that potential active sites on the catalyst surface can be localized by direct visualization of the outermost surface atoms basin. These atoms, similar to an atom in an isolated molecule, have considerable open parts that extend to infinity. Exposed atoms are open or unbounded at the exterior of the surface and a practical definition [37] is to cap these atoms with an isosurface of the electron density with small $\rho(\mathbf{r})$ value representing the van der Waals envelope of the system. A very efficient way to visualize and quantify the strength of the active sites is to map the electrostatic potential onto colors on this exterior atomic border [20]. In order to continue improving the understanding of HDS catalysts, in the present paper we have explored the nature of the active sites on the NiMoS catalyst using the combination of AIM and the electrostatic potential based methodology of Ref. [20].

2. The AIM theory

The topological properties of a crystal charge distribution are summarized by its critical points (CP) [29,38]. These are points where the gradient vector field, $\nabla\rho(\mathbf{r})$ vanishes, and they are classified by the $\rho(\mathbf{r})$ curvatures or three eigenvalues λ_i ($i = 1, 2,$ and 3) of the Hessian matrix ($H_{ij} = \partial^2\rho(\mathbf{r})/\partial x_i \partial x_j$). They are labeled by their rank (number of nonzero eigenvalues) and signatures (excess number of positive over negative eigenvalues) and correspond to maxima (3, −3), minima (3, +3), and saddle points (3, +1) and (3, −1). Every CP has a characteristic pattern of trajectories or gradient paths of $\rho(\mathbf{r})$. The trajectories originate and end at critical points. Only the (3, −3) points are three-dimensional trajectory attractors: trajectories only terminate at this CP. The (3, −3) points occur generally at the nuclear positions so that each nucleus is a three-dimensional point attractor in the vector field $\nabla\rho(\mathbf{r})$. The region traversed by the gradient paths, which terminate at a given attractor defines the *basin* of the attractor. A (3, −1) CP, the *bond critical point* (b), is found between every pair of neighboring nuclei. It represents both local maxima in two directions and a local minimum in the third direction. The gradient paths associated with the negative eigenvalues at the (3, −1) point terminate at this CP and define the interatomic surfaces, IAS, that partition the crystal into unique fragments (the *atomic basins*). In general, the boundary of an atom in a crystal consists of the union of its interatomic surfaces. The unique pair of trajectories associated with the positive eigenvalue of the (3, −1) CP originates at this point and terminate at the neighboring attractors. These two unique gradient paths define a line (the *bond path*) linking the nuclei (n), along which the charge density is a maximum with respect to any neighboring line. The network of bond paths defines a graph, namely the *crystal graph*, which describes the atomic connectivity and structure within a crystal cell. The other CPs occur as a consequence of the geometrical arrangements of bond paths and they define the remaining elements of crystal structure, namely rings and cages. If the bond paths are linked to form a ring of bonded atoms then a (3, +1) CP is found in the interior of the ring. The eigenvectors associated with the two positive eigenvalues of the (3, +1), a *ring* (r) CP, generate an infinite set of gradient paths which originate at the CP and define a surface, called the ring surface. All of these trajectories terminate at the ring nuclei or at the bond CPs whose bond paths form the perimeter of the ring. The single negative eigenvector of the ring CP generates a pair of gradient paths, which terminate at the CP and define a unique axis perpendicular to the ring surface at the critical point. The (3, +3) or *cage* (c) CPs are located inside a cage nuclear arrangement. The charge

density is a local minimum at a cage CP and in crystals it is the main source of trajectories of $\nabla\rho(\mathbf{r})$: trajectories only originate at such CPs and terminate at nuclei, bond or ring CPs. The type and numbers of CPs for an extended system [32,37] satisfy the Morse invariant relationships

$$n - b + r - c = 0 \tag{1}$$

3. The electrostatic potential methodology

Nature of active sites can be particularly explored using the electrostatic potential, $V(\mathbf{r})$, which let us directly to determine where the electron-rich sites in a molecule or crystal are localized [64–74]. $V(\mathbf{r})$ at a point $\mathbf{r}$ generated by a molecule or crystal is given by,

$$V(\mathbf{r}) = V_{\mathrm{N}}(\mathbf{r}) + V_{\mathrm{E}}(\mathbf{r}) \tag{2}$$

where the two terms $V_{\mathrm{N}}(\mathbf{r})$ and $V_{\mathrm{E}}(\mathbf{r})$ represent the bare nuclear and electronic contributions, respectively, to the total electrostatic potential. The sign of $V(\mathbf{r})$ at a given point indicates whether the nuclear (positive) or electronic (negative) effects are dominant. The electrostatic potential at $\mathbf{r}$ generated by the total charge distribution, ρ^{tot}, of a periodic system is given by,

$$V(\mathbf{r}) = \sum_n \int \rho^{\mathrm{tot}}(\mathbf{r}' - \mathbf{R}_n)|\mathbf{r} - \mathbf{r}'|^{-1}\,\mathrm{d}\mathbf{r}' \tag{3}$$

The summation extends to all direct lattice vectors, the prime on the integral sign indicating that an infinitesimal region about $\mathbf{r} = \mathbf{r}'$ is excluded from the domain of integration to avoid divergent nuclear self-interactions terms that would otherwise arise in the electrostatic energy per cell. ρ^{tot} may be decomposed into electronic and nuclear components,

$$\rho^{\mathrm{nuc}}(\mathbf{r}) = \sum_{\mathrm{a}} q_{\mathrm{a}}\delta(\mathbf{r}_{\mathrm{a}}, \mathbf{r}) \tag{4}$$

where the summation extends to all the reference cell nuclei, with atomic numbers and position vectors denoted q_{a} and $\mathbf{r}_{\mathrm{a}}$, respectively.

$$\rho^{\mathrm{el}}(\mathbf{r}) = -\sum_{ij}\sum_{\mu\nu} P_{\mu\mathbf{R}_i\nu\mathbf{R}_j}\chi_\mu(\mathbf{r} - \mathbf{R}_i)\chi^*_\nu(\mathbf{r} - \mathbf{R}_i) \tag{5}$$

where P is the density matrix and $\chi_\mu(r - \mathbf{R}_i)$ is the μ_{th} reference cell basis function translated by the direct lattice vector $\mathbf{R}_i$. The summations over i and j extend to all direct lattice vectors, while those over μ and ν include all the basis functions of the reference cell. Substitution of Eqs. (4) and (5) into Eq. (3) gives the nuclear and electronic $V(\mathbf{r})$ contributions.

For the region nearest to the nucleus V_{N} dominates and $V(\mathbf{r})$ has similar topology to the electron density [75,76], $\rho(\mathbf{r})$. i.e., positive-valued maxima at the nuclear site and a positive-valued saddle point between every pair of bonded atoms. Nevertheless, the existence of maxima is ruled out via an established result that, barring the nuclear position, there can not exist any strict local maxima in the $V(\mathbf{r})$ map [67,68]. For the region where V_{E} dominates ($V(\mathbf{r})$ is negative) the $V(\mathbf{r})$ topography can be more complex. However, it is well known that lone pairs of electrons as well as double π bonds (C=C, C=N, etc.) are generally characterized as negative valued minima [66,69]. In summary, the region nearest to the nucleus is always positive-valued while the region where the potential is negative-valued contains the minima that characterize the atom lone pairs. The minima of the negative region denote the zones to which an approaching electrophile may be attracted. On the contrary, the positive regions do not have maxima that might indicate sites for nucleophilic attack. Nevertheless, Politzer and Sjoberg have shown that by computing $V(\mathbf{r})$ on the 0.002-electron/bohr^3 contour isosurface [77] of the molecular electronic density $\rho(\mathbf{r})$, we can quantify the susceptibility of molecules to nucleophilic attack. They demonstrated that relative magnitudes of the positive electrostatic potential in various regions on this surface do reveal the sites most susceptible to nucleophilic attack. This contour isosurface for a group of diatomic molecules and for methane encompasses at least 95% of the electronic charge and yields physically reasonable molecular dimensions [77]. Mapping on this isosurface the $V(\mathbf{r})$ values onto colors let us to identify the host sites in which nucleophiles (most positive zone) and electrophiles (most negative zone) should bind. Additionally, the active sites susceptibility can be quantify determining the minimum and maximum $V(\mathbf{r})$ values at the determined host zones using a Newton-Raphson technique like to those that we have previously reported for the study of the electronic density [20,78] and electrostatic potential topology [73,74,79].

4. Computational methodology

$\rho(\boldsymbol{r})$ and $V(\boldsymbol{r})$ were calculated by means of the Dmol^3 [80,81] program using the Kohn-Sham Hamiltonian with the gradient-corrected Perdew-Becke-Ernzerhof (PBE) exchange-correlation functional [82]. Dmol^3 calculates variational self-consistent solutions to the DFT equations, expressed in an accurate numerical atomic orbital basis. The solutions to these equations provide the molecular electron densities, which can be used to evaluate the total electrostatic potential of the system. The numerical double-zeta plus polarization basis set *DNP* [80,81] was used in all calculations. DMol^3 uses DFT to obtain high accuracy while keeping the computational cost fairly low for an ab-initio method. Six special k points generated using a [4 3 1] mesh along the three cell axes and the Monkhorst-Pack scheme [80,81] were used to integrate the wavefunction in the reciprocal space. The topology of $\rho(\mathbf{r})$ was determined using a reported implementation [78] of the Newton-Raphson and fifth-order Cash-Karp Runge-Kutta methods in a $\rho(\mathbf{r})$ three-dimensional grid.

5. Catalyst models

STM allows direct imaging of catalytically relevant surface structure on the atomic scale. By studying [25] a realistic HDS model system consisting of few-nanometer-wide gold-supported MoS_2 particles it was shown that morphology of the nanoparticles is sensitive to sulfiding and reactions conditions, this means, triangles under heavy sulfiding conditions or truncated hexagons under more sulfo-reductive conditions resembling HDS conditions. These hexagonal clusters expose

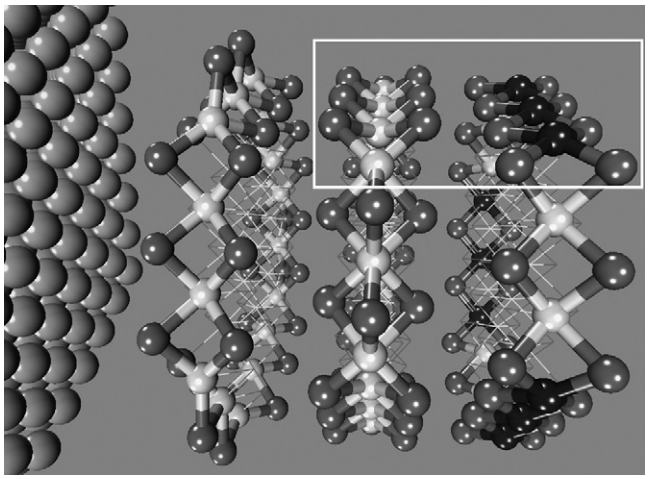

Fig. 1. Balls and cylinders model showing a side view of a hypothetical three-layer MoS_2 nanoparticle placed at the surface of the support (spheres at the left) that simulates the particles of Ref. [4]. White, gray and black spheres denote the Mo, S and Ni atoms on the edges, respectively. A white rectangle highlights the structure of the site that interacts with the incoming molecules. Right, center and left layers simulate a Mo edge promoted by three Ni atoms, an S edge and a non-promoted Mo edge, respectively.

the basal plane and two different types of edges: Mo edges covered with S monomers and fully-saturated S edges with H atoms adsorbed [25]. Different models have been used to study the edge structure of MoS_2 catalysts using DFT methods: cluster models including a finite number of atom [25,83], a single S–Mo–S periodic slab [84,85] and a larger slab model containing two S–Mo–S sheets exposing Mo- and S-edges alternatively [25,27,86–89]. From these studies a clear picture of the MoS_2 edge structures has emerged. The most external Mo atoms of the Mo edge contain 50% sulfur coverage with each sulfur atom bridged to two neighboring molybdenum atoms. A significant reconstruction of the Mo edge take places: the bridged S atoms are to be shifted by half a lattice constant relative to the bulk S lattice, and they move down to a bridging position in-plane with the Mo lattice. The S edges of the electronically most stable structure remain fully sulfide [88] and a maximum Mo coordination to six sulfur atoms is achieved in one configuration where the edge is terminated by a row of sulfur atoms positioned in bridge position close to those expected from bulk-terminated MoS_2. Both edge geometries lead to a coordination number of six for the outermost molybdenum atoms and two for the corresponding sulfur atoms. The local atomic structure of NiMoS catalysts has been resolved by means of DFT calculations coupled with simple thermodynamics determinations [17,27]. Under typical sulfidation conditions nickel prefers to incorporate into the metal edge in a square planar geometry with no sulfur atoms. On a partially promoted metal edge, sulfur atoms bond to the outermost Mo atoms and the Ni atoms tend to be uncovered [27]. High-resolution electron microscopy studies of silica-supported Mo based catalysts have shown that the morphology of the catalyst can be depicted as small particles dispersed at the surface of the support with an average size of 29 Å (mean diameter) and three slabs of wide. Fig. 1 shows a model of such as particle. The structure of the particle edge (the active site) is highlighted by means of a white square.

We have modeled these sites by means of the larger slab model (Fig. 2) that exposes alternating layers of Mo and S edges denoting nanoparticles several layers wide. The unit cell (9.480 Å × 12.294 Å × 36.000 Å) of the non-promoted surface exhibits three and six bridged S atoms on the Mo and S edges, respectively [20]. Partial substitution of one or two Mo atoms on the Mo-edge generated an edge structure, M(33), with 33% (Fig. 2a and b) and M(66) with 66% (Fig. 2c and d) Mo atoms substituted by Ni atoms, respectively. Substitution of the three Mo atoms on the Mo-edge generated an edge structure, M(1 0 0), with 100% Mo atoms substituted by the Ni atoms (Fig. 2e and f). The unit cells containing a periodic slab of several layers of atoms initially having the same structure of the surface built directly from the bulk. Vacuum layers thicker than 15 Å were used to ensure that there were no interactions between adjacent slabs. The geometry of those models was optimized using algorithms included in the Dmol^3 program [80,81]. The two upper rows were allowed to relax while the atoms of the lower ones were kept fixed at their optimized bulk positions to simulate bulk constrains.

6. Results

Atomic basins, i.e., the volume spanned by the paths ending at a given nucleus, are topologically equivalent to polyhedra, in the sense that they have faces, edges and vertexes, and they satisfy Eulerĭs relationship (faces − edges + vertexes = 2) [36]. Unlike polyhedra, however, basins tend to have rather curved edges and faces. Vertexes are cage CPs, edges are the attraction lines between cage and ring CPs and each face is the attraction surface of a bond CP, i.e., the IAS. A vision 3D of the metal-S IAS (white structure) defining the basin for the outermost atoms for M33 are given in Fig. 3. The basin for the outermost S atom (pointed by a white arrow) on the Mo edge, is bordered by two Mo–S interatomic surfaces. This atom, such as an atom in an isolated molecule [38], has considerable open parts that extend to infinity (Fig. 3b and c). A practical definition of open or unbounded atoms at the exterior is to cap the atom with an isosurface of the electron density with small $\rho(\mathbf{r})$ value representing the van der Waals envelope of the system [38]. The 0.007 electron/Å^3 contour of $\rho(\mathbf{r})$ shown in Fig. 3a just defines the border of the outermost atoms of the NiMoS edges. The basin for the outermost Mo atoms on the Mo-edge (Fig. 3d and e) is bordered by five Mo–S IAS, four shared with its closest S neighbors locate just below them and one shared with the outermost S atom that is locate above them. This later IAS corresponds just to a half of the outermost sulfur atom base and almost covers and encapsulates the Mo atoms. The basin for the Ni atom (Fig. 3f and g) is bordered by four Ni–S IAS and likes to the outermost S atom is open to the exterior of the NiMoS edges. Thus, the outermost atoms of the NiMoS edges are mainly defining by metal–sulfur interatomic surfaces. A recently study of the MoS_2 edges has shown that direct visualization of the structure and shape of the basin of these metal–sulfur IAS allow us to locate the Lewis acid site (the CUS) on the surface edges [20]. In the same way, Fig. 4 shows a top view of super-cells for the studied NiMoS edge models. As we can see, similar to the non-promoted MoS_2

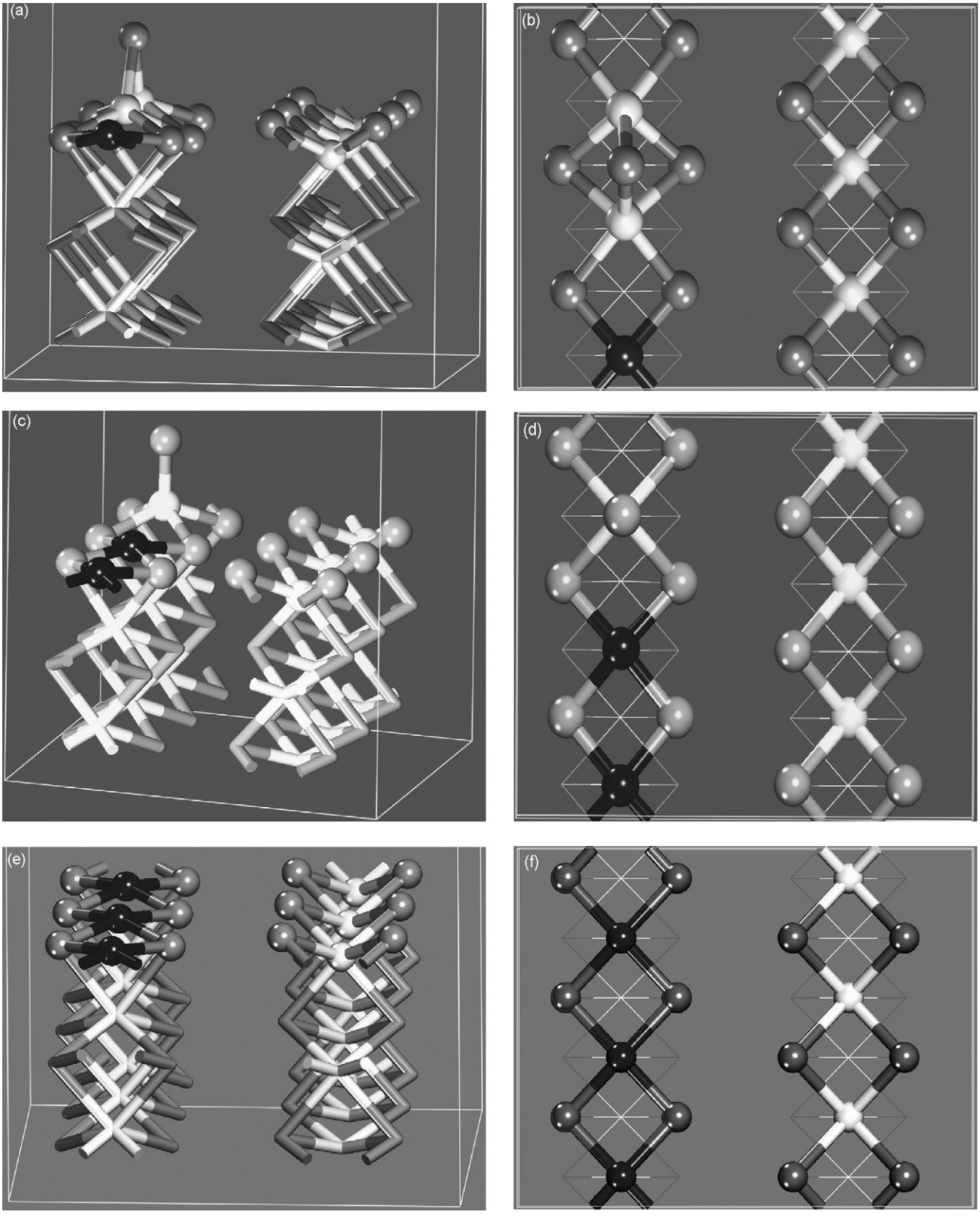

Fig. 2. (Left) Top-view (*XZ* plane) and (right) side-view (*YZ* plane) of the NiMoS edges unit cell. M33 (a and b), M66 (c and d) and M100 (e and f) contain one, two and three Ni atoms by cell, respectively. White, gray and black spheres denote the Mo, S and Ni atoms, respectively. The S edges are on the right of each unit cell and expose six S atoms by cell.

catalyst, the Mo atoms are mainly covered by the outermost sulfur atoms which obstruct the Mo interaction with the pollutant sulfur (or nitrogen) atoms on the incoming molecules (pyridine, thiophene, dibenzothiophene, etc.). The basins for the outermost S atoms on the S edges show exactly the same structure and shape of the corresponding atoms of the un-promoted MoS_2 edges. Thus, the metal atoms most accessible to the exterior of the edges are the Ni atoms (dark blue spheres).

HDS susceptibility of the sites on the exposed atoms can be particularly explored mapping the electrostatic potential on the $\rho(\mathbf{r})$ isosurface capping them [20]. This mapping allows us to identify the host sites in which nucleophiles (most positive zone) and electrophiles (most negative zone) should bind. Additionally, the local maximum value of $V(\mathbf{r})$ at the determined host zones provides a quantitative determination of the Lewis acidity strength on the outermost atoms. For the non-promoted MoS_2 catalyst [79], a site obtained by removing three S atoms from the cell, just on the S edge, with 50% of sulfur coverage was suggested to be the HDS potential active site. A hole in the IAS defining the outermost S atoms corresponds to the site where the Mo atoms are most accessible to the incoming molecules. Located at this hole, a $V(\mathbf{r})$ maximum on the $\rho(\mathbf{r})$ isosurface with a value of 51.982 kJ/mol was determined [79]. A top view of the $V(\mathbf{r})$ color maps for the NiMoS Mo-edge models studied in the present paper are shown in Fig. 5. A double cell along to the Mo edge is showed. One cell shows the superposition of the color map on the exposed atoms basins of the Mo-edge while the other cell only shows the $V(\mathbf{r})$ color map. Starting from the most negative $V(\mathbf{r})$ values (see caption of Fig. 5), three kinds of blue and three kinds of green denote the most negative ones while

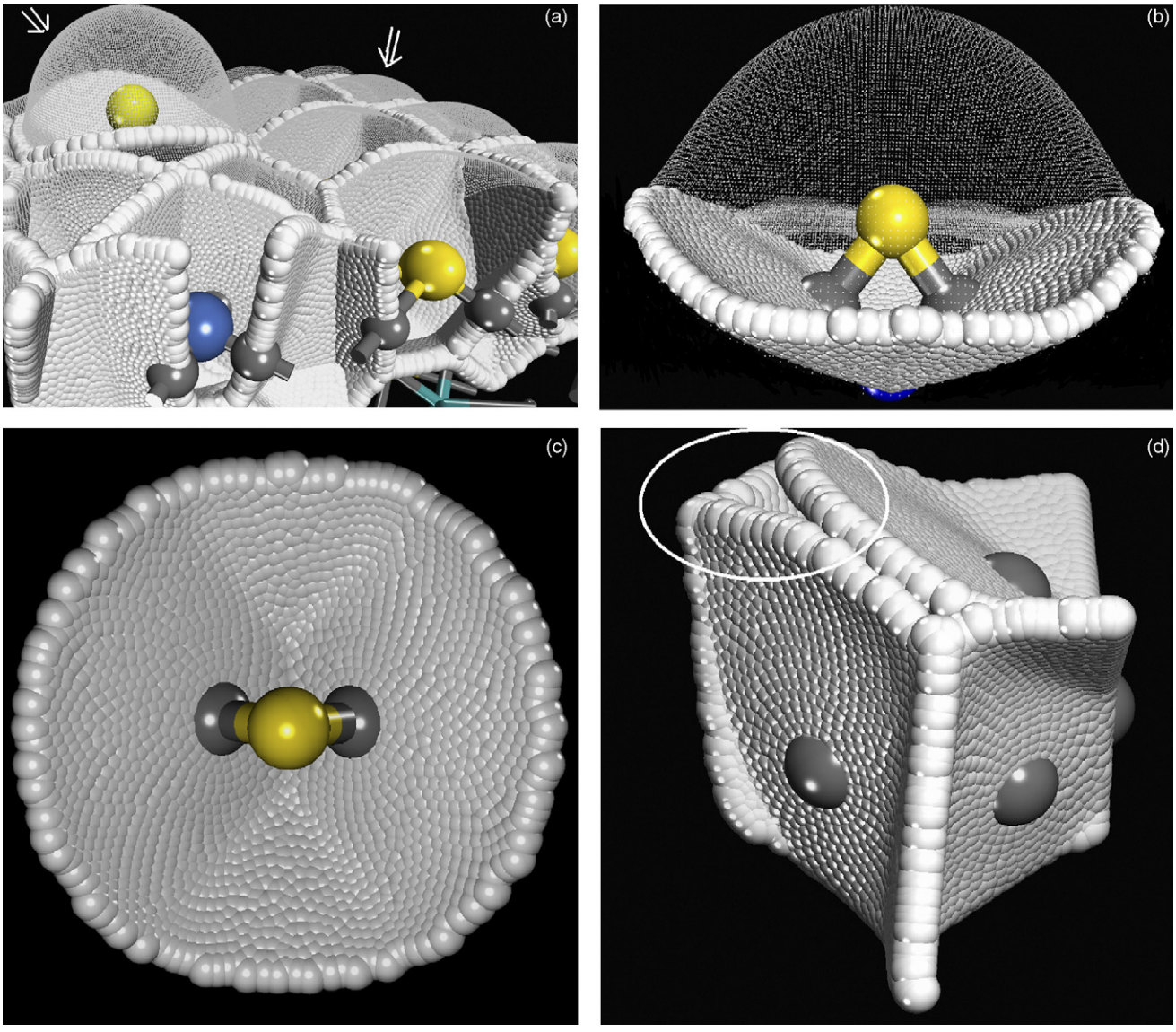

Fig. 3. (a) Side-view of the atomic basins for the outermost atoms on M33 defined by the metal–sulfur IAS (white structures). Note that these atoms are open system and a practical definition is to cap them with an isosurface (pointed by a white arrow) of $\rho(\mathbf{r})$. (b) Side-view and (c) Top-view of the IAS defining the basin of the outermost S atoms on the Mo edge. (d)–(g) Corresponding views of the outermost Mo and Ni basin on the Mo edge, respectively. Gray spheres denote metal–sulfur bond CPs, respectively. Light blue, and yellow spheres denote Ni and S atoms, respectively. The Mo atoms are almost covered by the S atoms. White ellipses highlight the small atom region open to the exterior. (For interpretation of the references to color in this figure legend, the reader is referred to the web version of the article.)

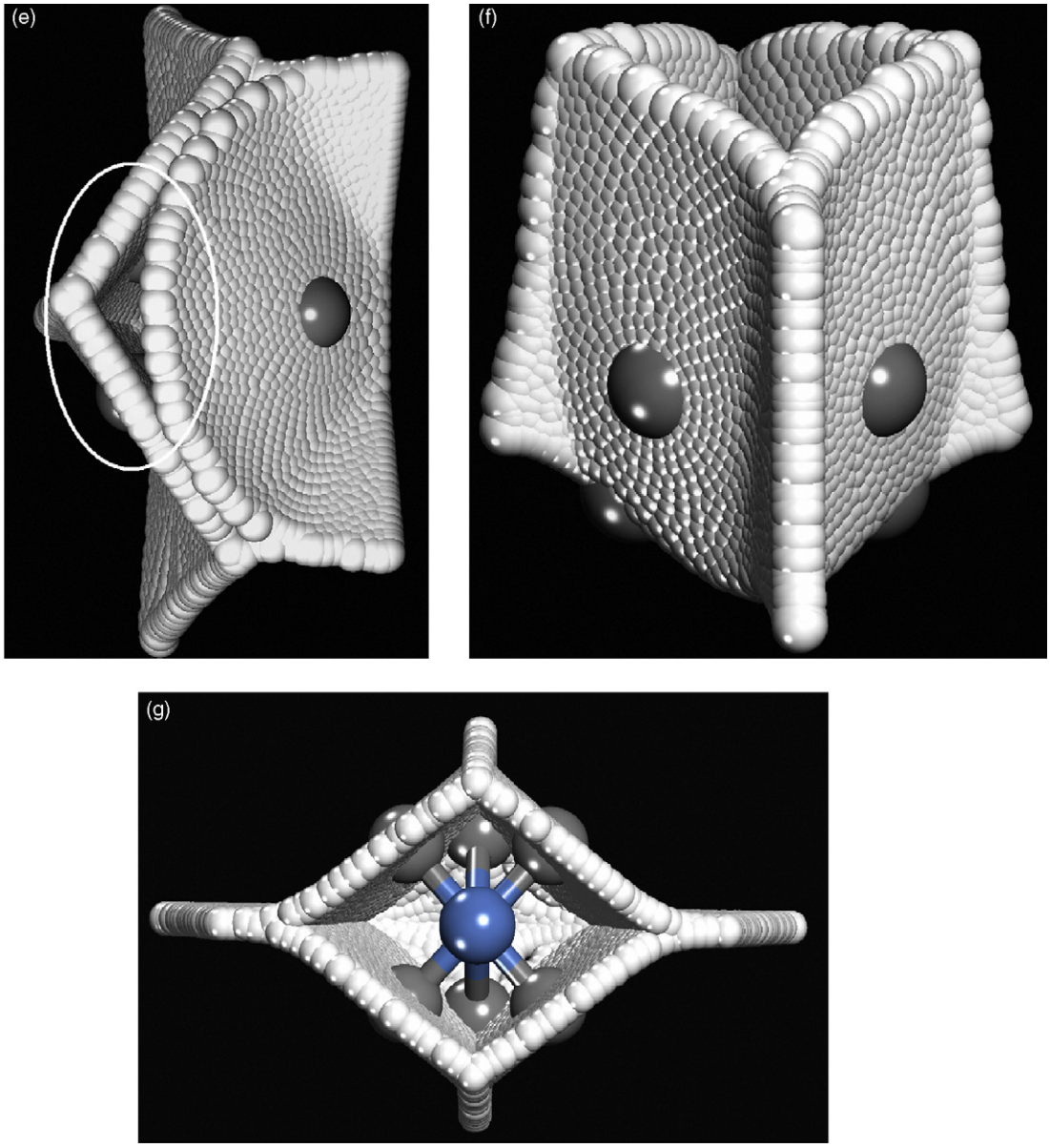

Fig. 3. (*Continued*).

two kinds of yellows, one orange, one brown, one purple and two kinds of red denote the positive $V(\mathbf{r})$ values. M33 (Fig. 5a) exhibits small areas of red zones (highlighted by black ellipses) localized at both sides of the Mo basin, just at small holes in the IAS that define the outermost S atom. These red zones are the most positive sites on M33. Purple zones (pointed by black arrows) at the Ni atoms suggest that these atoms are less acid than the Mo atoms. Fig. 5b suggests that all the atoms of M66

Table 1
Maximum positive value of $V(\mathbf{r})$ and vacancy creation energy, CE (Eq. (7)) for the studied sites on the metallic edges of the NiMo sulfide

Ni coverage	$V(\mathbf{r})$ maximum (kJ/mol) on $\rho(\mathbf{r}) = 0.002$ e/A^3	Located at	$V(\mathbf{r})$ maximum (kJ/mol) on $\rho(\mathbf{r}) = 0.007$ e/A^3	Located at
100% (Fig. 5a)	45.946	Ni	81.391	Ni
66% (Fig. 5b)	27.305	Ni	66.688	Ni
33% (Fig. 5c)	52.773	Mo	94.781	Mo

Ni coverage	CE (kJ/mol)	$V(\mathbf{r})$ maximum (kJ/mol) on $\rho(\mathbf{r}) = 0.002$ e/A^3	Located at	$V(\mathbf{r})$ maximum (kJ/mol) on $\rho(\mathbf{r}) = 0.007$ e/A^3	Located at
One sulfur atom removed					
66% (Fig. 8)	168.300	137.314	Mo	210.303	Mo
33%	250.649	119.723	Mo		Mo

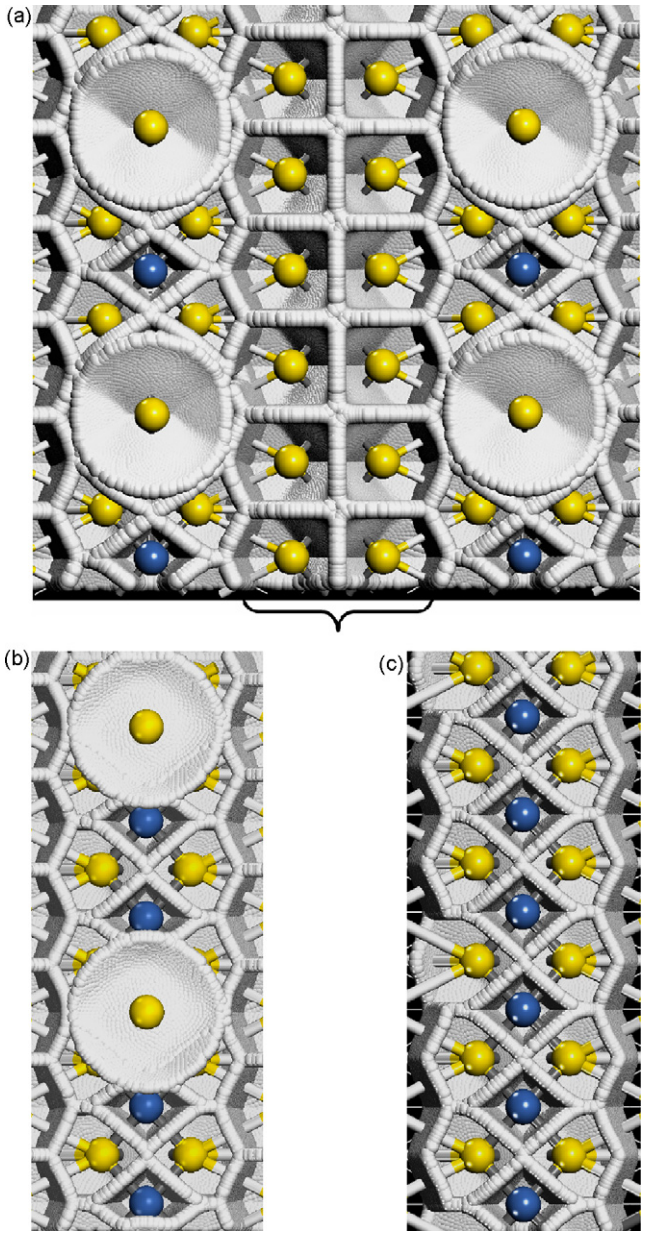

Fig. 4. Top-view of the M33 (a), M66 (b) and M100 (c) surface periodic model showing the IAS defining the basins of the outermost atoms. Dark blue and yellow spheres denote Ni and S atoms, respectively. In (a) an S edge (highlighted by a black brace) with two Mo edges at both sides is showed, while (b) and (c) only show just one Mo edge. Note that the Mo atoms are practically encapsulated by the outermost S atoms. (For interpretation of the references to color in this figure legend, the reader is referred to the web version of the article.)

are less acid than M33. Negative green zones cover the outermost S atoms which in turn totally cover the Mo atoms, while brown zones (less positive than the purple one) are localized on the Ni atoms. Fig. 5c shows a purple zone on each Ni atom of M100 suggesting that the Lewis acidity of these atoms increase with regard to the corresponding atoms of M66 and it make no difference with M33.

The determined $V(\mathbf{r})$ maxima values by Mo-edge cell are presented in Table 1. These values are reported for the mapping on two $\rho(\mathbf{r})$ isosurfaces, $\rho(\mathbf{r}) = 0.002$ and $\rho(\mathbf{r}) = 0.007$ e/Å^3. This later isosurface (0.001 au) can be considered as the practical outer limit of the atoms in molecules, crystals or surfaces; because, in general, it encompasses at least 95% of the electronic charge of the system [38]. However, any $\rho(\mathbf{r})$ isosurface closest to 0.007 e/Å^3 leads to same deductions: the maxima (or minima) are exactly at the same place. The $V(\mathbf{r})$ value at these maxima depends on the $\rho(\mathbf{r})$ isosurface value: in general, $V(\mathbf{r})$ increase as the $\rho(\mathbf{r})$ isosurface value increase and the isosurface is closer to the atomic nuclei. However, in a series of molecules or surfaces, the $V(\mathbf{r})$ maxima show exactly the same trends. Thus, the obtained trends for both isosurfaces is,

$$\rho(\mathbf{r}) = 0.007\,\text{e/Å}^3\text{:}\quad \text{Mo}_{\text{-M33}}\,(94.781) > \text{Ni}_{\text{-M33}}\,(79.815) \approx \text{Ni}_{\text{-M100}}\,(81.391) > \text{Ni}_{\text{-M66}}\,(66.688),$$

$$\rho(\mathbf{r}) = 0.002\,\text{e/Å}^3\text{:}\quad \text{Mo}_{\text{-M33}}\,(52.773) > \text{Ni}_{\text{-M33}}\,(45.421) \approx \text{Ni}_{\text{-M100}}\,(45.946) > \text{Ni}_{\text{-M66}}\,(27.305).$$

These results suggest that the most Lewis acidity sites (the most positive one) on the NiMoS edge models are localized on the M33 Mo atoms. The Ni atom for M33 and M100 should exhibit almost the same acidity, while for M66 the acidity of the Ni atoms appreciably decreases. M100 and M66 should be less acid than non-promoted MoS_2 catalyst ($V(\mathbf{r})_{max} = 51.982$ kJ/mol on the $\rho(\mathbf{r})$ isosurface = 0.002 e/Å^3) and the most acid site at M33 should be similar acid than the non-promoted MoS_2 edges. However, an appreciable improves of the Lewis acidity strength was reported for the promoted catalyst system using FTIR spectroscopy [4] and DFT theoretical study [90] with pyridine, PY, as the probe molecule. On non-promoted catalyst and a CoMoS phase, PY adsorption rise to bands at 1600 (of low intensity) and 1609 (of high intensity) cm^{-1}, respectively [4]. In agreement with this experimental results, DFT calculations of the adsorption energy of a pyridine molecule on periodic models of non-promoted [79] and on the M100 Ni-edge [90] have reported values of 88.852 and 124.466 kJ/mol, respectively. From this trend it is evident that in the adsorption of PY on the NiMoS edges other additional features should be considered. Therefore, we have explored the binding of PY on the three studies models, using Dmol^3 again. A PY molecule was placed inside the surface unit cell, on the considered metal atom, aligned as the $V(\mathbf{r})$ map predicts. The geometry was fully optimized to their most energetically favorable positions, maintaining fixed the two innermost layers at the bottom of the cell. The predicted geometries are shown in Fig. 6 and the trend of binding energy, BE, obtained was,

$$\text{M100}\,(128.650\,\text{kJ/mol}) > \text{M33}\,(108.696\,\text{kJ/mol}) > M66\,(57.971\,kJ/mol)$$

The smaller BE was found for M66, where the nitrogen atom of PY is adsorbed on top of a Ni atom with a bond distance nitrogen–nickel, $Re_{N–Ni}$ of 2.752 Å. The nitrogen atom is just at the side of an outermost S atom doing an interatomic distance nitrogen–sulfur, $Re_{N–S}$ of 3.582 Å. For M33, an increase around of 100% in BE with respect to M66 was obtained. PY

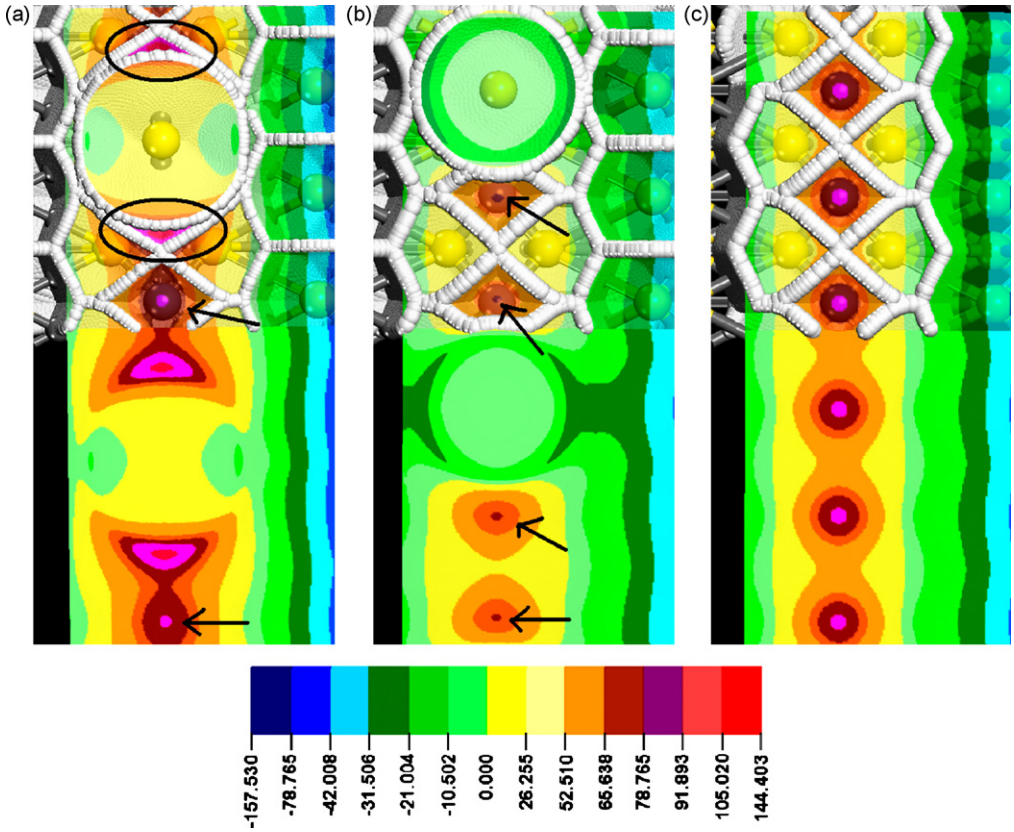

Fig. 5. Top view of the $V(\mathbf{r})$ mapping on the 0.007 au contour of $\rho(\mathbf{r})$ defining the outermost border of the Mo edge exposed atoms for (a) M33, (b) M66 and (c) M100. A double cell along to the Mo edge is showed. One cell shows the superposition of the color map on the exposed atoms basins of the Mo-edge while the other cell only shows the $V(\mathbf{r})$ color map. The tab at the bottom is, blue jay (−157.530 to −78.765 kJ/mol), blue heaven (−78.765 to −42.008 kJ/mol), light blue (−42.008 to −31.506 kJ/mol), dark green (−31.506 to −21.004 kJ/mol), green (−21.004 to −10.502 kJ/mol), light green (−10.502 to 0.000 kJ/mol), yellow (0.000 to 26.255 kJ/mol), yellow cream (26.255 to 52.510 kJ/mol), orange (52.510 to 65.638 kJ/mol), brown (65.638 to 78.765 kJ/mol), purple (78.765 to 91.893 kJ/mol), light red (91.893 to 105.020 kJ/mol) and red (105.020 to 144.403 kJ/mol). Black arrows pointed to the Ni atoms while black ellipses highlight the small Mo regions exhibited to the exterior of the edge. (For interpretation of the references to color in this figure legend, the reader is referred to the web version of the article.)

is adsorbed atop of the only Ni atom of the cell, with $Re_{N–Ni}$ and $R_{N–S}$ equals to 2.030 and 4.825 Å, respectively. For M33, the access to the most acidity site which is located at the Mo atom is not allowed for the outermost S atoms. An additional increases of 18% in BE was determined for M100 where PY also adsorbs on top of a Ni atom with $Re_{N–Ni} = 1.994$ Å. To further examine these findings, we have studied the $V(\mathbf{r})$ color maps $\rho(\mathbf{r}) = 0.002$ e/Å^3 for the interaction of the PY molecule with M66 and M33 and the results are shown in Fig. 7. For PY a negative zone embraces the nonbonding region of the N atom (blue zone) with a minimum value (denotes as a white square in Fig. 7) of −115.522 kJ/mol while a negative zone (green zone) with a local minimum of −12.864 kJ/mol covers the M66 outermost sulfur atom (Fig. 7a). Repulsion between both negative regions impedes the free access to the Lewis acid sites (denote as white arrows). The outermost S atoms for M33 (Fig. 7b) show a light green zone with a local minimum of −5.536 kJ/mol just at the center of the atom. This smaller minimum and the presence of a positive valley between the outermost S atoms allow a comfortable interaction with the N negative blue zone of PY. From these results it is evident that the N atom of PY has a tendency to adsorb at sites where the repulsive nitrogen-outermost S interaction is minimized. Thus, the PY adsorption strongly depends on two factors: the Lewis acidity of the site and the repulsive interaction of the N atom with S atoms impeding the free access to the site. PY binding on a site like to M100 containing an uncovered by sulfur atoms site with $V(\mathbf{r})_{max} = 45.946$ kJ/mol shows an increase of 18% and 45%, respect to M33 and the non-promoted MoS_2 edges [79], that contain obstructed Lewis acid sites with $V(\mathbf{r})_{max}$ of 52.773 and 51.982 kJ/mol, respectively. In this sense, the main role of the promoter is to produce uncovered Lewis acid sites.

The effect on the stability of the non-promoted MoS_2 edge surface of the reaction conditions such as temperature and partial pressure of H_2 and H_2S present in the surrounding atmosphere has been reported [88], using a combination of periodic DFT calculations and thermodynamic analysis. It was found that the sulfur coverage of both kinds of edges is strongly dependent on the H_2S/H_2 partial pressure ratio in the surrounding gas phase. For high pressure of H_2S the surface with six sulfur atoms at the S edge is the most stable surface. For high hydrogen pressure, that should correspond to the catalyst working conditions, the surface with 50% sulfur coverage (three sulfur vacancies by cell) at the S edge, AS, should be the most stable surface. Vacancies or CUS are created by a reduction process where H_2 reacts with exposed sulfur atoms to produce H_2S and therefore, the energy

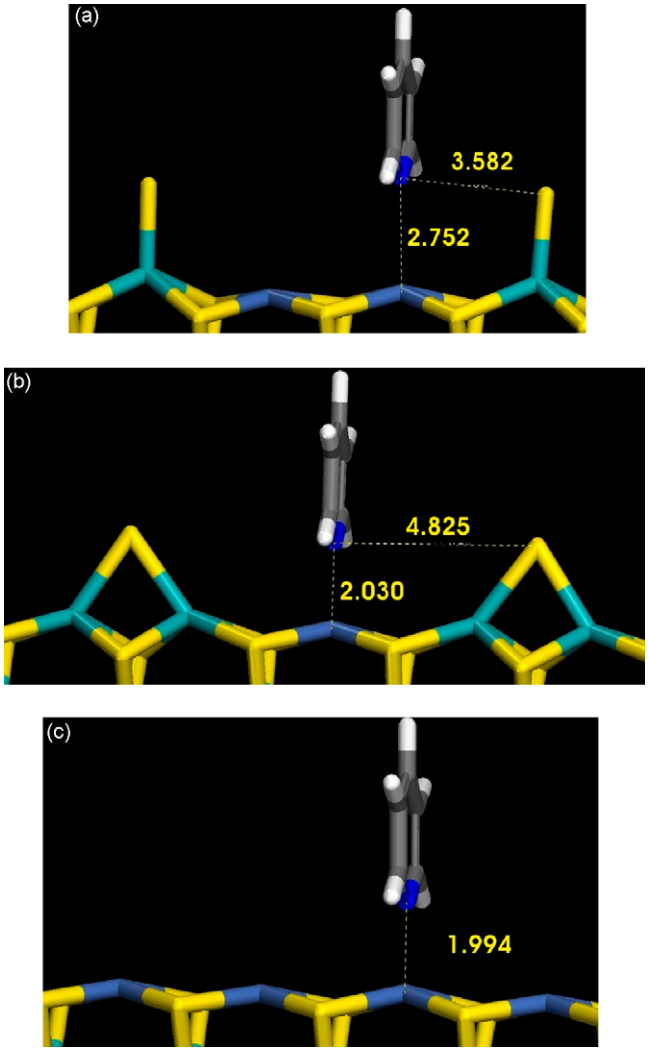

Fig. 6. Cylinders model for the adsorption optimized geometry (distances in Å) of a pyridine molecule adsorbed on M66 (a), M33 (b) and M100 (c). Light blue, dark blue and yellow cylinders denote Mo, Ni and S atoms for the NiMoS edge model, while dark blue, gray and white cylinders denote the N, C and H atoms of the pyridine molecule. (For interpretation of the references to color in this figure legend, the reader is referred to the web version of the article.)

to create a sulfur vacancy can be calculated using the following equilibrium:

$$\text{Surface-S} + H_2 \Leftrightarrow \text{Surface-}\square + H_2S. \quad (6)$$

Thus, the creation energy, CE, of a sulfur vacancy is given by the expression:

$$CE = E(\text{Surface-}\square) + E(H_2S) - E(\text{Surface-S}) - E(H_2) \quad (7)$$

Removal of three S atoms on the sulfur edge to create the non-promoted AS only needs 72.579 kJ/mol while removal of just one S atom on the Mo edge costs 153.345 kJ/mol [79]. In spite of this thermodynamic result, kinetic modeling [89] of H_2S removal from the edge surfaces has shown that is possible to extract one S atom per Mo edge creating a very small number of vacancy/cell on this edge. However, the previous study [79] of the MoS_2 edge vacancies Lewis acidity strength has shown that just one CUS on the Mo edge creates weak Lewis acid sites,

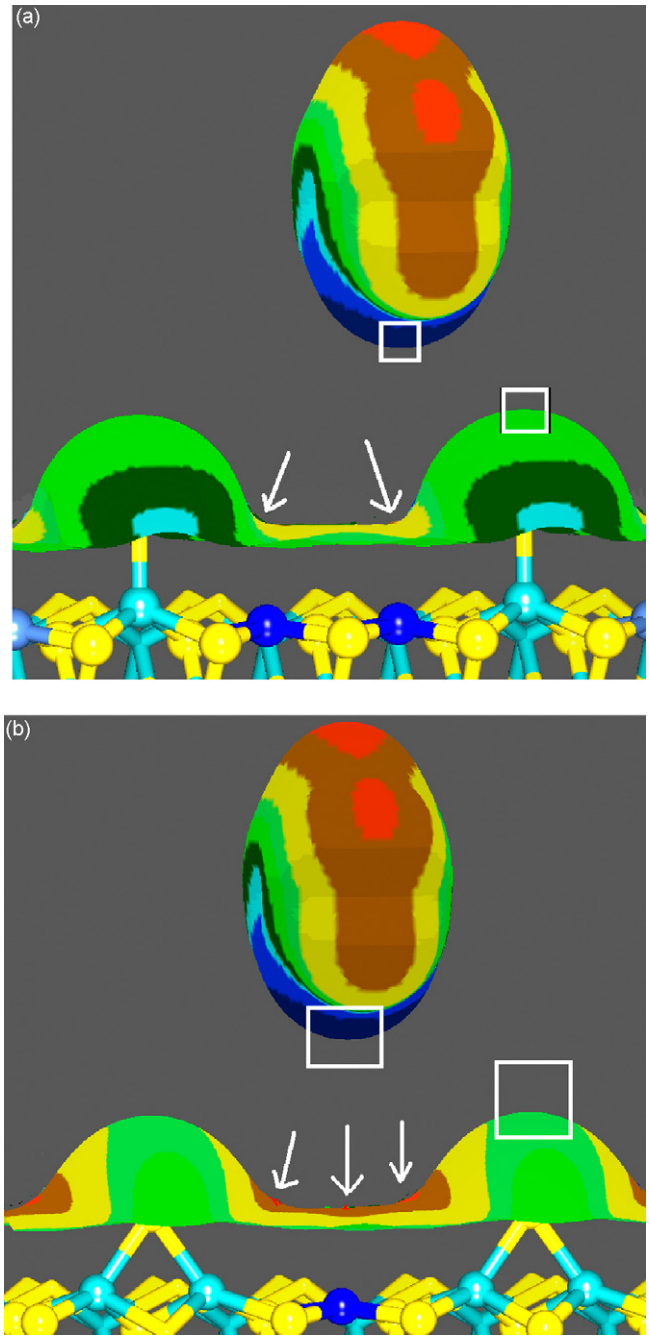

Fig. 7. Side view of the $V(\mathbf{r})$ mapping on the 0.007 au contour of $\rho(\mathbf{r})$ defining the outermost border of the pyridine molecule adsorbed on the Mo edge exposed atoms for (a) M66 and (b) M33. The color tab is the same of Fig. 5. White arrows point to the strongest Lewis acid sites while, white square highlight the most negative sites at the pyridine N atom and the outermost S atoms. (For interpretation of the references to color in this figure legend, the reader is referred to the web version of the article.)

even weaker than AS. In order to obtain very acid sites at least two atoms have to be removed at the Mo edges, but to a cost of a huge (271.810 kJ/mol) creation energy. These results confirm the presence of available weak Lewis acidic sites on the non-promoted MoS_2 catalyst such as AS at the catalytic reaction conditions. In the present work, we have studied the removal of the outermost S atom for M33 and M66 using Eq. (7) and the

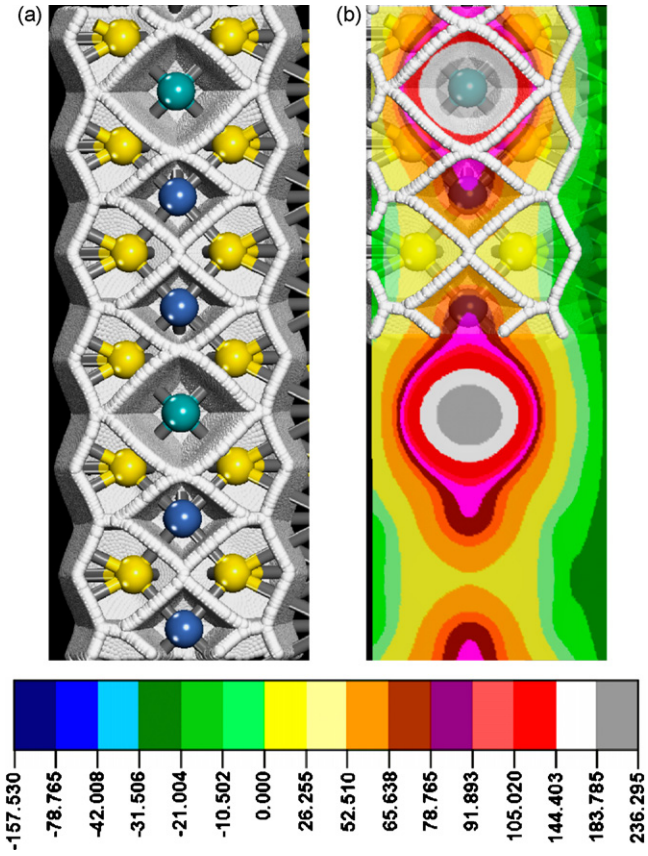

Fig. 8. (a) Top-view of the Mo edge of M66_uncov surface periodic model with the outermost S atoms extracted to create uncovered Mo atoms showing the IAS defining the basins of the outermost atoms. Dark blue, light blue, and yellow spheres denote Ni, Mo and S atoms, respectively. (b) Top view of the $V(\mathbf{r})$ mapping on the 0.007 au contour of $\rho(\mathbf{r})$ defining the outermost border of the Mo edge exposed atoms for M66_uncov. A double cell along to the Mo edge is showed. One cell shows the superposition of the color map on the exposed atoms basins of the Mo-edge while the other cell only shows the $V(\mathbf{r})$ color map. The tab at the bottom additionally includes white (144.403 to 183.785 kJ/mol) and brown (183.785 to 236.295 kJ/mol) zones. (For interpretation of the references to color in this figure legend, the reader is referred to the web version of the article.)

obtained CEs are also listed in Table 1. M33 and M66 contain 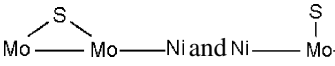 sites. For M66, the energy cost (168.30 kJ/mol) for creating a totally uncovered sulfur site, $M66_{unconv}$, corresponds to an increase of only 10% of the corresponding cost (153.345 kJ/mol) to extract an S atom on the non-promoted Mo edge. However, different to the non-promoted catalysts, $M66_{unconv}$ (see Fig. 8) contains very strong Lewis acid sites with $V(\mathbf{r})_{max} = 137.314$ kJ/mol on $\rho(\mathbf{r}) = 0.002$ e/Å^3. If similar for the non-promoted MoS_2, the extraction of a sulfur atom on the Mo edge is possible then a strong Lewis acid site like to $M66_{unconv}$ will be present at the particles edge of the NiMoS catalyst. TDS, XPS and hydrogen-chemisorption studies [28a] and Ab initio DFT study of hydrogen dissociation on NiMoS including mechanism, kinetics and vibrational frequencies [28d] have found that H_2 could dissociate on the Ni sites and move to react with S centers and form a S vacancy. Thus, in general, we can conclude that the main role of the Ni atoms is to make possible the formation of uncovered metal sites at the Mo edges of the MoS_2 nanocrystallites and the most Lewis acid sites should be located at Ni–Mo–Ni sites containing uncovers Mo atoms.

7. Concluding remarks

Direct visualization of the basin of the outermost atoms of the studied NiMoS edge models has shown that the Mo atoms are practically covered by the outermost S atoms while the promoter Ni are the most accessible atoms to the exterior of the edges. $V(\mathbf{r})$ mapping on the $\rho(\mathbf{r})$ isosurface capping the outermost edge atoms and adsorption of pyridine as the probe molecule have shown that the adsorption of a molecule containing the pollutant atoms strongly depends on two factors: the Lewis acidity of the site and the repulsive interaction of the incoming molecule with outermost sulfur atoms impeding the free access to the site. In this sense, the main role of the promoter is to produce sulfur uncovered Lewis acid sites. To obtain very strong Lewis acidic sites, the outermost S atom has to be extracted to create uncovered Mo atoms located at Ni–Mo–Ni sites.

References

[1] O. Weisser, S. Landa, Sulfide Catalysts: Their Properties and Applications, Pergamon, Oxford, UK, 1973.
[2] H. Topsoe, B.S. Clausen, F.E. Massoth, Hydrotreating Catalysis Science and Technology, vol. 11, Springer Verlag, Berlin, 1996.
[3] J.A. Rodriguez, J. Dvorak, A.T. Capitano, A.M. Gabelnick, J.L. Gland, Surf. Sci. 429 (1999) L462–L468.
[4] G. Berhault, M. Lacroix, M. Breysse, F. Maugé, J.-C. Lavalley, H. Nie, L. Qu, J. Catal. 178 (1998) 555–565.
[5] M. Breysse, G. Berhault, S. Kasztelan, M. Lacroix, F. Maugé, G. Perot, Catal. Today 66 (2001) 13–20.
[6] R. Pis Diez, A.H. Jubert, J. Mol. Catal. 83 (1993) 219–325.
[7] (a) J.K. NØrskov, B.S. Clausen, H. TopsØe, Catal. Lett. 13 (1992) 1–8; (b) H. TopsØe, B.S. Clausen, N.-Y. TopsØe, J.K. NØrskov, C.V. Ovesen, C.J.H. Jacobsen, Bull. Soc. Chim. Belg. 104 (1995) 283.
[8] (a) H. Toulhoat, G. Kresse, Am. Chem. Soc. Div. Petrol. Chem. Prepr. 42 (1997) 114; (b) H. Toulhoat, P. Raybaud, S. Kasztelan, G. Kresse, J. Hafner, Catal. Today 50 (1999) 629–636.
[9] (a) T.A. Pecoraro, R.R. Chianelli, J. Catal. 67 (1981) 430–445; (b) R.R. Chianelli, G. Berhault, P. Raybaud, S. Kasztelan, J. Hafner, H. Toulhoat, Appl. Catal. A: Gen. 227 (2002) 83–96.
[10] R.R. Chianelli, M. Daage, M.J. Ledoux, Adv. Catal. 40 (1994) 117–232.
[11] S. Harris, R.R. Chianelli, J. Catal. 86 (1984) 400–412; H. Toulhoat, P. Raybaud, J. Catal. 216 (2003) 63–72.
[12] J.P.R. Vissers, C.K. Groot, E.M. Vanoers, V.H.J. de Beer, Bull. Soc. Chim. Belg. 93 (1984) 813–821.
[13] M.J. Ledoux, O. Michaux, G. Agostini, P. Panisso, J. Catal. 102 (1986) 275–288.
[14] J.K. Burdett, J.T. Chung, Surf. Sci. Lett. 236 (1990) L353–L357.
[15] T.S. Smith, K.H. Johnson, Catal. Lett. 28 (1994) 361.
[16] P. Raybaud, G. Kresse, J. Hafner, H. Toulhoat, J. Phys.: Condens. Matter 9 (1997) 11085–11106.
[17] P. Raybaud, J. Hafner, G. Kresse, S. Kasztelan, H. Toulhoat, J. Catal. 190 (2000) 128–143.
[18] M. Neurock, R.A. van Santen, J. Am. Chem. Soc. 116 (1994) 4427–4439.
[19] Y. Aray, J. Rodriguez, D. Vega, E.N. Rodriguez-Arias, Angew. Chem. Int. Ed. 39 (2000) 3810–3813.
[20] Y. Aray, J. Rodriguez, J. Mol. Catal. A: Chem., in press.
[21] B.S. Clausen, B. Lengeler, R. Candia, J. Als-Nielsen, H. Topsoe, Bull. Soc. Chim. Belg. 90 (1981) 1249–1259.

[22] T.G. Parham, R.P. Merrill, J. Catal. 85 (1984) 295–310.
[23] S.J. Tauster, T.A. Pecoraro, R.R. Chianelli, J. Catal. 63 (1980) 515–519.
[24] H. Topsoe, R. Candia, N.Y. Topsoe, B.S. Clausen, Bull. Soc. Chim. Belg. 93 (1984) 783–806.
[25] (a) J.V. Lauritsen, M.V. Bollinger, E. Lægsgaard, K.W. Jacobsen, J.K. Nørskov, B.S. Clausen, H. Topsøe, F. Besenbacher, J. Catal. 221 (2004) 510–522;
(b) H. Schweiger, P. Raybaud, H. Toulhoat, J. Catal. 212 (2002) 33–38;
(c) P. Raybaud, J. Hafner, G. Kresse, S. Kasztelan, H. Toulhoat, J. Catal. 189 (2000) 129–146;
(d) H. Schweiger, P. Raybaud, G. Kresse, H. Toulhoat, J. Catal. 207 (2002) 76–87.
[26] R. Prins, V.H.J. de Beer, G.A. Somorjai, Catal. Rev.-Sci. Eng. 31 (1989) 1–41.
[27] (a) M. Sun, J. Adjaye, A.E. Nelson, Appl. Catal. A: Gen. 263 (2004) 131–143;
(b) M. Sun, J. Adjaye, A.E. Nelson, J. Catal. 226 (2004) 32–40.
[28] (a) J.A. Rodriguez, S.Y. Li, J. Hrbek, H.H. Huang, G.-Q. Xu, Surf. Sci. 370 (1997) 85;
(b) J.A. Rodriguez, J. Phys. Chem. B 101 (1977) 7524;
(c) M. Sun, A. Nelson, J. Adjaye, Catal. Today 105 (2005) 36;
(d) M. Sun, Adjaye, J. Catal. 233 (2005) 411.
[29] (a) R.F.W. Bader, Atoms in Molecules-q Quantum Theory, Clarendon Press, Oxford, UK, 1990;
(b) R.F.W. Bader, Chem. Rev. 91 (1991) 893.
[30] R.F.W. Bader, J. Phys. Chem. A 102 (1998) 7314–7323.
[31] R.F.W. Bader, P.L.A. Popelier, T.A. Keith, Angew. Chem. Intl. Ed. Eng. 33 (1994) 620–631.
[32] P.F. Zou, R.F.W. Bader, Acta Crystallogr. A50 (1994) 714–725.
[33] M.E. Eberhart, J. Can. Chem. Soc. 74 (1996) 1229.
[34] M.E. Eberhart, Philos. Mag. A 73 (1996) 47.
[35] Y. Aray, J. Rodriguez, D. Vega, J. Phys. Chem. B 104 (2000) 4608.
[36] M.A. Pendás, A. Costales, V. Luaña, Phys. Rev. B 55 (1997) 4275.
[37] P. Popelier, Atoms in Molecules—An Introduction, Prentice Hall, Harlow-England, 2000.
[38] R.J. Gillespie, P.L.A. Popelier, Chemical Bonding and Molecular Geometry: From Lewis to Electrón Densities, Oxford University Press, New York, Oxford, 2001.
[39] N.E. Ghermani, C. Lecomte, Y. Dusausoy, Phys. Rev. B 53 (1996) 4231.
[40] C.L. Hénaff, N.K. Hansen, J. Protas, G. Marnier, Acta Crystallogr., B 53 (1997) 870.
[41] Y.V. Ivanov, E.L. Belokoneva, J. Protas, N.K. Hansen, V.G. Tirelson, Acta Crystallogr. B 54 (1998) 774.
[42] T.S. Koritsanszky, P. Coppens, Chem. Rev. 101 (2001) 1583.
[43] R.T. Downs, G.V. Gibbs, M.B. Boisen Jr., K.M. Rosso, Phys. Chem. Miner. 29 (2002) 369.
[44] Y.A. Abramov, F.P. Okamura, Acta Crystallogr. A 53 (1997) 187.
[45] M. Takata, M. Sakata, S. Kumazawa, F.K. Larsen, B. Iversen, Acta Crystallogr. A 50 (1994) 330.
[46] S.F. Vyboishchikov, A.E. Masunov, V.A. Streltsov, P.M. Zorkii, V.G. Tirelson, Zh. Fiz. Khim. 68 (1994) 2024.
[47] R. Boese, A.D. Boese, D. Blazer, M.Y. Antipin, A. Ellern, K. Seppelt, Angew. Chem. Int. Ed. Engl. 36 (1997) 1489.
[48] R. Boese, N. Niederprum, D. Blazer, A. Maulitz, M.Y. Antipin, P.R. Mallison, J. Phys. Chem. B 101 (1997) 5794.
[49] P. Munshi, T.N. Guru Row, Crystallogr. Rev. 11 (2006) 199.
[50] C.J. Mei, K.E. Edgecombe, V.H. Smith, A. Heilingbrunner, Int. J. Quantum Chem. 48 (1993) 287.
[51] Y. Aray, J. Rodríguez, J. Rivero, J. Phys. Chem. A 101 (1997) 6976.
[52] P. Mori-Sánchez, Densidad electrónica y enlace químico, De la molécula al cristal, Ph.D. Thesis, Universidad de Oviedo, 2002.
[53] M.E. Eberhart, D.P. Clougherty, J.M. MacLaren, J. Am. Chem. Soc. 115 (1993) 5762.
[54] M.E. Eberhart, D.P. Clougherty, J.M. MacLaren, J. Mater. Res. 8 (1993) 438.
[55] U. Haussermann, S. Wengert, R. Nesper, Angew. Chem. Int. Ed. Engl. 33 (1994) 2073.
[56] G.H. Grosch, K.J. Range, J. Alloys Compd. 233 (1996) 39.
[57] M. Knecht, H. Ebert, W. Bensch, J. Alloys Compd. 246 (1997) 166.
[58] V.G. Tirelson, P. F: Zou, T.H. Tang, R.F.W. Bader, Acta Crystallogr. A 51 (1995) 143.
[59] C. Gatti, V.R. Saunders, C. Roetti, J. Chem. Phys. 101 (1994) 10686.
[60] J.A. Plats, S.T. Howard, J. Chem. Phys. 105 (1996) 4668.
[61] V. Luaña, A. Costales, P. Mori-Sánchez, M.A. Pendás, J. Phys. Chem. B 107 (2003) 4912.
[62] M.A. Blanco, A. Costales, A.M. Pendás, V. Luaña, Phys. Rev. B 62 (2000) 12028.
[63] M.A. Pendás, A. Costales, V. Luaña, Phys. Rev. B 55 (1997) 4285.
[64] M. Leboeuf, M. Koster, K. Jug, D.R. Salahub, J. Chem. Phys. 111 (1999) 4893.
[65] S.R. Gadre, R.N. Shirsat, Electrostatics of Atoms and Molecules, Universities Press, Hyderabad, 2000.
[66] (a) S.S. Pingale, S.R. Gadre, L.J. Batolotti, J. Phys. Chem. A 102 (1998) 9987;
(b) M.M. Deshmukh, N.V. Sastry, S.R. Gadre, J. Chem. Phys. 121 (2004) 12402;
(c) K.A. Joshi, S.P. Gejji, J. Mol. Struct. Theochem. 724 (2005) 87;
(d) H. Tachikawa, T. Iyama, H. Kawabata, J. Mol. Struct. Theochem 718 (2005) 117.
[67] (a) R.K. Pathak, S.R. Gadre, J. Chem. Phys. 93 (1990) 1770;
(b) S.R. Gadre, S.A. Kulkarni, I.H. Shrivastava, J. Chem. Phys. 96 (1992) 5253.
[68] S.R. Gadre, R.K. Pathak, Proc. Ind. Acad. Sci. (Chem. Sci). 102 (1989) 18.
[69] (a) C. Alhambra, F.J. Luque, M. Orozco, J. Phys. Chem. 99 (1995) 3084;
(b) P. Kornelak, A. Michalak, M. Najbar, Catal. Today 101 (2005) 175;
(c) A. Michalak, Chem. Phys. Lett. 386 (2004) 346.
[70] P. Politzer, D.G. Truhlar, Chemical Applications of Atomic and Molecular Electrostatic Potentials, Plenum, New York, 1982.
[71] J.S. Murray, K.D. Sen, Molecular Electrostatic Potential: Concepts and Applications, Elsevier, Amsterdam, 1996.
[72] M. Orozco, F.J. Luque, Theor. Comput. Chem. Ser. 3 (1996) 181.
[73] Y. Aray, M. Marquez, J. Rodríguez, S. Coll, Y. Simón-Manso, C. Gonzalez, D.A. Weitz, J. Phys. Chem. B 107 (2003) 8946.
[74] (a) Y. Aray, M. Marquez, J. Rodríguez, S. Coll, Y. Simón-Manso, C. Gonzalez, D.A. Weitz, J. Phys. Chem. B 108 (2004) 2418;
(b) Y. Aray, J. Rodríguez, S. Coll, C. Gonzalez, M. Marquez, J. Phys. Chem. B 108 (2004) 18942.
[75] Y. Tal, R.F.W. Bader, J. Erkku, Phys. Rev. A 21 (1980) 1.
[76] T.A. Keith, R.F.W. Bader, Y. Aray, Int. J. Quant. Chem. 57 (1996) 183.
[77] P. Sjoberg, P. Politzer, J. Phys. Chem. 94 (1990) 3959.
[78] Y. Aray, J. Rodriguez, D. Vega, in: C.F. Matta, R.J. Boyd (Eds.), The Quatum Theory of Atoms in Molecules: From DNA to Solid and Drug Design, Wiley–VCH, Weinheim, in press.
[79] Y. Aray, J. Rodriguez, S. Coll, E. Rodríguez-Arias, D. Vega, J. Phys. Chem. B 109 (2005) 23564–23570.
[80] $DMol^3$ is available as part of Material Studio. Accelrys Inc., San Diego, USA, 2002.
[81] B. Delley, J. Chem. Phys. 92 (1990) 508;
B. Delley, J. Chem. Phys. 113 (2000) 7756.
[82] J.P. Perdew, K. Burke, M. Emzerhof, Phys. Rev. Lett. 77 (1996) 3865.
[83] L.S. Byskov, J.K. Norskov, B.S. Clausen, H. Topsoe, Catal. Lett. 64 (2000) 95.
[84] L.S. Byskov, J.K. Norskov, B.S. Clausen, H. Topsoe, Catal. Lett. 47 (1997) 177.
[85] L.S. Byskov, J.K. Norskov, B.S. Clausen, H. Topsoe, J. Catal. 187 (1999) 109.
[86] P. Raybaud, J. Hafner, H. Kresse, H. Toulhoat, Phys. Rev. Lett. 80 (1998) 1481.
[87] P. Raybaud, J. Hafner, H. Kresse, H. Toulhoat, Surf. Sci. 407 (1998) 237.
[88] S. Cristol, J.F. Paul, E. Payen, D. Bougeard, F. Clemendot, F. Hutschka, J. Phys. Chem. 104 (2000) 11220.
[89] J.F. Paul, E. Payen, J. Phys. Chem. B 107 (2003) 4057.
[90] M. Sun, A. Nelson, J. Adjaye, J. Catal. 231 (2005) 223.